Journal of Materials Chemistry A

Accepted Manuscript

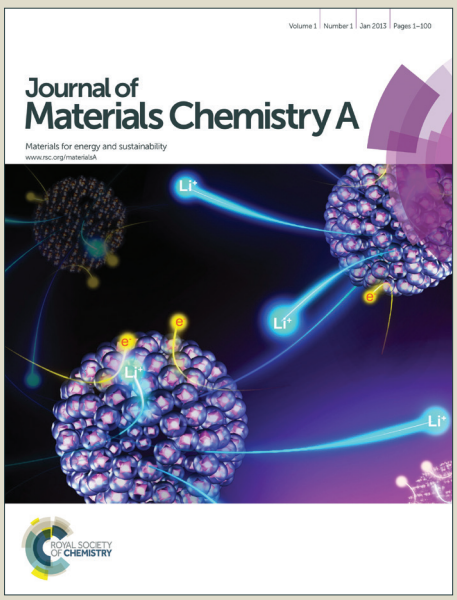

ROYAL SOCIETY OF CHEMISTRY

www.rsc.org/materialsA

Journal of Materials Chemistry A RSCPublishing

ARTICLE

Plasma enhanced atomic layer deposition of Fe_2O_3 thin films

Cite this: DOI: 10.1039/xoxxoooooox

Ranjith K. Ramachandran, Jolien Dendooven, and Christophe Detavernier*

Received ooth January 2012,
Accepted ooth January 2012

DOI: 10.1039/xoxxoooooox

www.rsc.org/

Atomic layer deposition of Fe_2O_3 is generally performed at temperatures above 350 °C. In this work, Fe_2O_3 thin films were deposited by remote plasma enhanced atomic layer deposition using tertiary butyl ferrocene (TBF) and O_2 plasma in a broad temperature range starting from 150 to 400 °C. A maximum growth rate of 1.2 Å/cycle was achieved between 300 and 350 °C. Below 300 °C, the saturated growth per cycle was found to depend on the temperature of the sample. All the deposited films were pure with no significant amount of carbon contamination. Films deposited at 250 °C and above were crystalline with an α-Fe_2O_3 crystal structure, while the low temperature films were crystallized by a post-deposition annealing in He. Annealing in H_2 induced the formation of metallic iron.

Introduction

Hematite (α-Fe_2O_3) is the most common form of oxide in the Fe–O_2 system. Its unique combination of stability, nontoxicity and exceptionally low material cost makes it an important candidate for many applications such as magnetic devices[1–5], hydrocarbon gas sensors[6–9], photo electrochemical solar cells[10–15], heterogeneous catalysis[16–19], and as electro chromic material for smart windows[20,21].

Fe_2O_3 thin films have been grown for various purposes by a variety of different methods such as sputtering[1,22], sol-gel[4,7], molecular beam epitaxy (MBE)[23–25], metal organic deposition (MOD)[26,27], spray pyrolysis[20,28], chemical vapor deposition (CVD)[5,15,29–31] and atomic layer deposition (ALD)[8,32–40]. Amongst these methods, ALD is the most powerful method for depositing highly uniform and conformal layers, which is an important requirement for coating nanostructured surfaces. There exist several ALD processes for depositing iron oxide. While the first demonstrated tris-(2,2,6,6-tetramethyl-3,5-heptanedionato)iron(III) ($Fe(thd)_3$) and ozone process[32] suffers from an exceptionally low growth rate, the processes that use iron(III)tert-butoxide($Fe_2(O^tBu)_6$)[33,34] and bis(2,4-methylpentadienyl)iron[35] are limited by their narrow temperature window and commercial unavailability of the precursors. Most of the other methods use ferrocene ($Fe(Cp)_2$) as Fe precursor in combination with either molecular oxygen or ozone[36–39]. These processes generally use high deposition temperatures[36–38] (above 350 °C) while also suffering from extremely low growth rates[37] and narrow temperature windows for controlled growth[38]. Recently, Martinson et al.[39] reported an ALD process for Fe_2O_3 using $Fe(Cp)_2$ and O_3 in a lower temperature range from 200 to 350 °C with a crystalline phase starting from 250 °C. However, relatively large exposures of both $Fe(Cp)_2$ and O_3 are required to reach saturated growth conditions on planar surfaces.

In this article, we report a novel ALD process for Fe_2O_3 that relies upon sequential pulsing of ter-Butyl ferrocene (TBF) and O_2 plasma and allows for the controlled deposition of pure films in a broad temperature range from 150 to 350 °C. TBF is a commercially available liquid with a boiling point of 96 °C (at 1 mmHg) and with sufficient vapor pressure, which makes it a suitable precursor for ALD applications. In comparison with most existing ALD processes for Fe_2O_3, this novel process enables deposition at temperatures as low as 150 °C, which is attractive for applications that require the controlled deposition of iron oxide on temperature sensitive materials. Furthermore, the formation of metallic iron by a post deposition annealing of the films in H_2 is also demonstrated, which makes this novel process more versatile in view of technological applications such as data storage[41], surface plasmon coupled chemiluminescence[42,43], and biomedicine and magnetic devices[44].

Experimental details

All the depositions were performed in a home built experimental cold-wall ALD chamber connected through a gate valve to a turbo pump backed up by a rotary pump[45,46]. A second gate valve was installed for pre-evacuation of the chamber via a bypass line to the rotary pump. The liquid TBF precursor (98%, Strem Chemicals), kept in a stainless steel container, was heated to 65 °C, and the delivery line to the chamber was heated to 70 °C. For the remote plasma process the O_2 gas flowed through the plasma source at a pressure of 0.03 mbar and the RF plasma power was set at 300 W. The precursor was injected through a quarter inch stainless steel tube located at the top of the ALD chamber and a static

Department of Solid State Sciences, COCOON, Ghent University, Krijgslaan 281/S1, 9000 Ghent, Belgium,
E-mail: Christophe.detavernier@ugent.be, Phone: +32 9 264 4354, Fax: +32 9 264 4996

exposure mode was applied[47]. Unless stated otherwise, the pulse time of the TBF precursor was 15 s, after which the valves to the pumping system were kept closed for another 10 s, resulting in a total exposure time of 25 s at 1 mbar pressure. For O_2 plasma, the pulse time was 15 s. No purge gas was used in the deposition cycle.

The thickness of the growing Fe_2O_3 films was monitored in situ using spectroscopic ellipsometry (SE, J. A. Woollam M-2000). Based on SE measurements performed on several Fe_2O_3 layers with a known thickness, the optical constants of the films were found to be appropriately described by a Tauc-Lorentz oscillator model in the wavelength range of 600 to 1000 nm. Good quality fits to the ellipsometric data were obtained, even during the start of the film growth. The determination of film thickness by in situ SE was complemented by ex situ X-ray reflectivity (XRR) and X-ray fluorescence measurements. XRR was carried out using a Bruker D8 Discover system with Cu Kα radiation, while XRF was performed using a Mo x-ray source (at an angle of 45° with sample surface) and a silicon drift detector placed at an angle of 52° with the sample surface. The fluorescence signal was integrated over a period of 100s. Film thicknesses were extracted as explained in the Supporting Information.

The chemical composition of the deposited films was determined by X-ray photoelectron spectroscopy (XPS) using a Thermo VG Scientific ESCALAB 220i-XL with a monochromatic Al Kα x-ray source. The reported Binding Energy values (BE) were corrected for charging effects by assigning a BE of 284.6 eV to the C1s signal. The film crystallinity was investigated by X-ray diffraction (Bruker D8 Discover, Cu Kα radiation) using a point sensitive detector. The diffraction patterns were analyzed with the Scherrer equation to derive the size of the crystallites in the deposited films. The surface roughness of the films was determined by atomic force microscopy (AFM) on a Bruker Dimension Edge system operating in tapping mode in air. The Root Mean Square (RMS) roughness values were calculated on 5 µm x 5 µm micrographs.

The ALD process was characterized by in situ mass spectrometry (Hiden Analytical) using the spectrometer in Bar Scan mode with the Faraday detector (source voltage 70 V).

Finally, post-annealing of the deposited films in He and 5% H_2/He was performed in a home-built heating chamber mounted on a Bruker D8 diffractometer[48,49] to enable in situ XRD characterization. A linear detector was used to collect the diffracted X-rays at 2 s time intervals.

Results and discussion

Characteristics of the Iron Oxide ALD process

The temperature window of the ALD process was investigated on Si substrates covered with 100 nm thermally grown SiO_2. Figure 1 shows the variation in growth per cycle (GPC) with the temperature of the substrate. The substrate temperature was varied between 150 and 400 °C. The GPC has both temperature dependent and temperature independent regions. In the temperature range of 300 to 350 °C the GPC is temperature independent with a value of 1.2 Å/cycle. Below 300 °C the growth rate was found to decrease with decreasing temperature. Above 350 °C, the growth rate increased significantly, likely due to thermal decomposition of the TBF precursor. The thickness of the films deposited at and above 350 °C was extracted from XRF measurements (see Supporting Information)

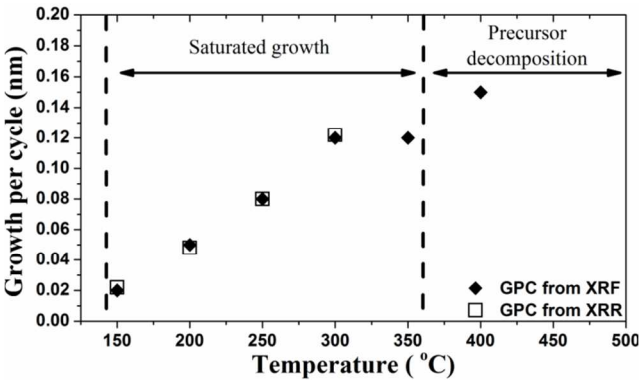

Figure 1. Growth rate as a function of deposition temperature.

Saturation of the ALD process was studied at different deposition temperatures. While both ALD half reactions saturate in the range of 150°C to 350 °C, no saturated growth was found at 400 °C, indicating thermal decomposition of the precursor at this temperature. Figures 2 (a) and (b) show the 150 and 300 °C saturation curves for the TBF precursor and O_2 plasma half cycles respectively. The pulse time of the TBF precursor was followed by an additional 10 s static exposure. At 300 and 350 °C a 7 s TBF pulse, resulting in a pressure of 7×10^{-1} mbar in the chamber, was sufficient to have saturated growth. However, at low temperatures, long pulse times were needed to ensure saturation. At the lowest deposition temperature of 150 °C a 15 s TBF pulse, resulting in a pressure of 1 mbar, was required for saturated growth. In the case of O_2 plasma, a 6 s exposure resulted in saturated growth at 300 °C, while 15 s were needed at 150 °C.

To get more insights in the mechanisms driving the temperature dependent saturation of the growth rate in the TBF/O_2 plasma process, in situ mass spectrometry was used to analyze the reaction products formed during both ALD half cycles. As also reported for the ferrocene/O_2 process by J.R. Scheffe et al.[37], CO_2 and H_2O were detected during both the precursor and reactant pulse. The formation of CO_2 and H_2O during the first half reaction indicates the presence of chemisorbed oxygen on the surface that reacts with the TBF ligands upon precursor adsorption. In the subsequent exposure to O_2 plasma, the remaining ligands of the adsorbed precursor molecules are oxidized[39,50–52]. Mass spectrometry revealed no difference in reaction products for the processes at 150 °C and 300 °C respectively, suggesting that similar ligand combustion reactions occur at both temperatures. The reduced growth rate at low temperatures could possibly be due to competing site blocking reactions by organic precursor groups during the TBF pulse. Surface poisoning by precursor fragments followed by removal of the surface carbon during the O_2 reactant step has earlier been proposed to occur during Pt and Ru ALD processes using Cp-based precursors[53].

The linearity of the ALD process was studied on 100 nm SiO_2 films thermally grown on Si substrates. The thickness after each ALD cycle was followed with in-situ spectroscopic ellipsometry measurements. Independent of the deposition temperature, there was a delay in the nucleation of the Fe_2O_3

film. The growth was limited up to about 30 cycles after which the film thickness increased linearly with the number of ALD cycles (Figure 3). The final thickness of the film was measured ex-situ with XRR and was in close agreement with the ellipsometric measurement.

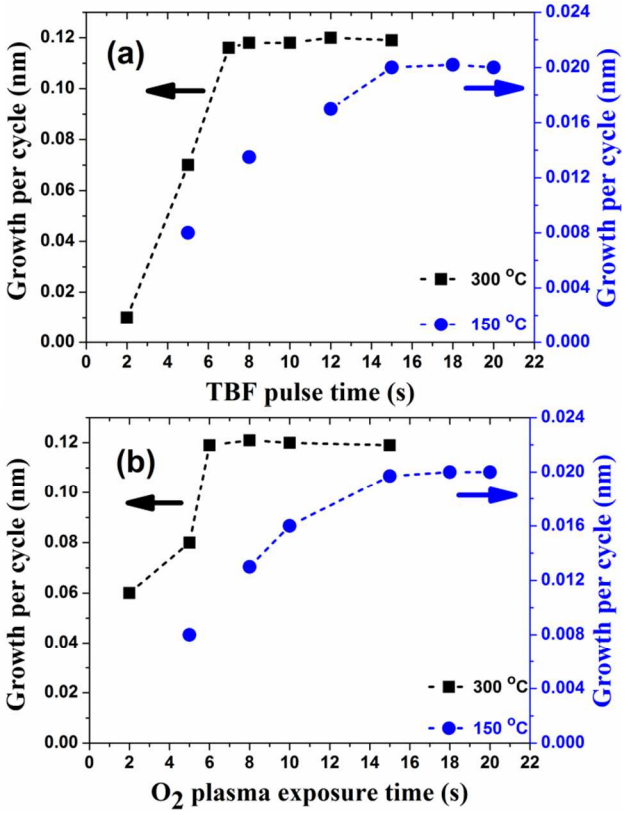

Figure 2. (a) Growth rate against the TBF pulse time, using a fixed O_2 plasma exposure of 15 s. **(b)** Growth rate against the O_2 plasma exposure time, using a fixed TBF total exposure of 25 s. The black squares were obtained at 300 °C (left Y-axis) and the blue circles at 150 °C (right Y-axis).

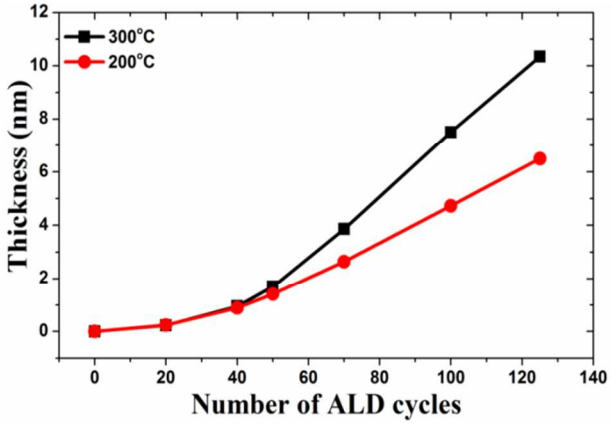

Figure 3. Thickness of the Fe_2O_3 films deposited at 200 and 300 °C on SiO_2 substrates against the number of ALD cycles. Ellipsometric measurements at certain intervals only are shown for clarity.

Properties of the Iron Oxide Films

Iron oxide films were deposited on 100 nm SiO_2/ Si substrates using the conditions described in the experimental section. All the deposited films were continuous and the thickness uniformity was excellent, with a typical deviation in thickness of less than 2% across a two-inch area. Phase identification of ca. 27 nm thick films was performed using XRD measurements. All the films deposited at and above 250 °C were crystalline and the XRD peaks correspond to an α-Fe_2O_3 (Hematite) phase (Figure 4). Analysis of the (104) peak with the Scherrer equation yielded crystallite sizes of 16 and 45 nm for the as deposited films at 250 °C and 350 °C respectively. The 3+ oxidation state of iron (Fe^{3+}) was also confirmed by XPS measurements. Figure 5 shows the XPS spectra of as-deposited films at 150 and 350 °C. The maximum of the Fe $2p_{3/2}$ peak is at 711 eV and the satellite peak between the $2p_{3/2}$ and $2p_{1/2}$ peaks is clearly visible. To verify the stoichiometry of the films, the O 1s peaks were studied in detail. Irrespetive of the deposition temperature, the O1s spectrum was characterized by the presence of two contributing bands.While the band at BE = 530.2 eV(species I, black, 74% of total oxygen content) could be ascribed to lattice oxygen in Fe_2O_3, the band at 532.2 eV (species II, gray) could be related to the presence of surface hydroxyl groups along with coordinatively unsaturated oxygen species[31,54]. Taking only the lattice oxygen species in to account the Fe/O ratio was found to be 0.62, in agreement with the stoichiometry expected for Fe_2O_3. Comparing these observations with those reported in literature[8,31,37,54,55], it can be concluded that the iron in the ALD films is in the Fe^{3+} state. XPS also showed a negligible amount of carbon (< 5%) in the deposited films.

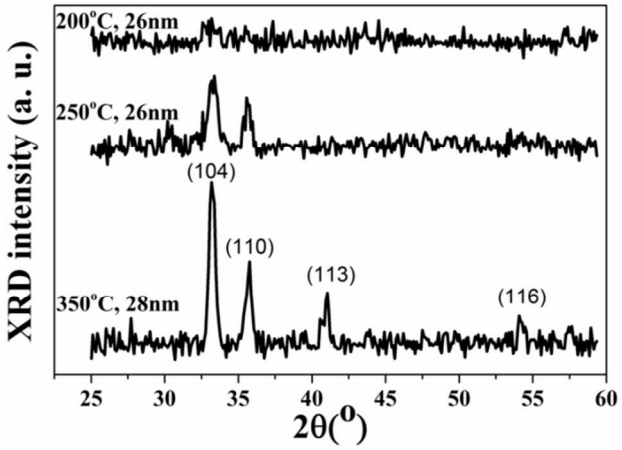

Figure 4. XRD patterns of the Fe_2O_3 films deposited at different temperatures on SiO_2 substrates.

All the films deposited below 250 °C were amorphous, but could be converted into the hematite phase with (104) preferential orientation by annealing in He. Figure 6 (bottom) shows the XRD patterns for the as-deposited film at 200 °C and for the same film annealed in He to 600 °C at a heating rate of 0.2 °C/s. The Figure 6 (top) shows the evolution of the XRD pattern during this thermal treatment. Crystallization of the film started at 350 °C, as revealed by the intensification of the peak corresponding to α-Fe_2O_3 (104). The Scherrer equation revealed an average crystallite size of 35 nm.

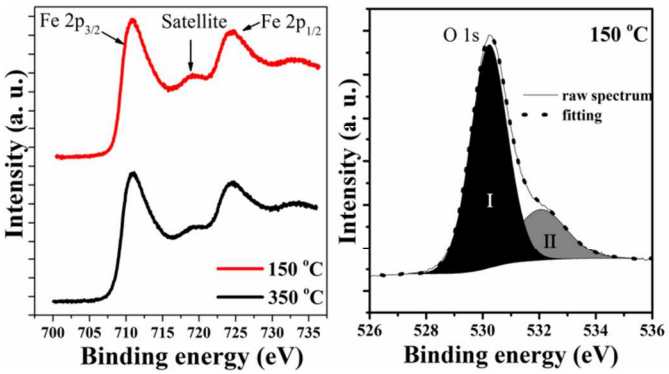

Figure 5. XPS spectra of Fe 2p (left) from the surface of Fe_2O_3 films deposited at 150 and 350 °C and O 1s (right) from the surface of Fe_2O_3 films deposited at 150 °C on SiO_2 substrates.

All the deposited Fe_2O_3 films can be reduced to metallic Fe by annealing in H_2 atmosphere. Upon annealing from room temperature to 650 °C at a heating rate of 0.2 °C/s, the Fe_2O_3 first reduces to Fe_3O_4 at 385 °C and then suddenly reduces to metallic Fe at 430 °C (Figure 7). This reduction process could be of interest for applications of metallic ferromagnetic iron in in data storage[41], biomedicine and magnetic devices[44].

Finally, the morphology of the films was studied using atomic force microscopy (AFM). As also reported for the iron(III) chloride and water process[40], the surface roughness of the Fe_2O_3 films was found to increase with increasing deposition temperature (Figure 8). This increase in surface roughness is related to the higher crystallinity of the films with increasing temperature. The rms roughness of the film deposited at 200 °C, which was measured from a 5 µm x 5 µm scan area, increased from 0.32 to 0.81 nm after annealing in He.

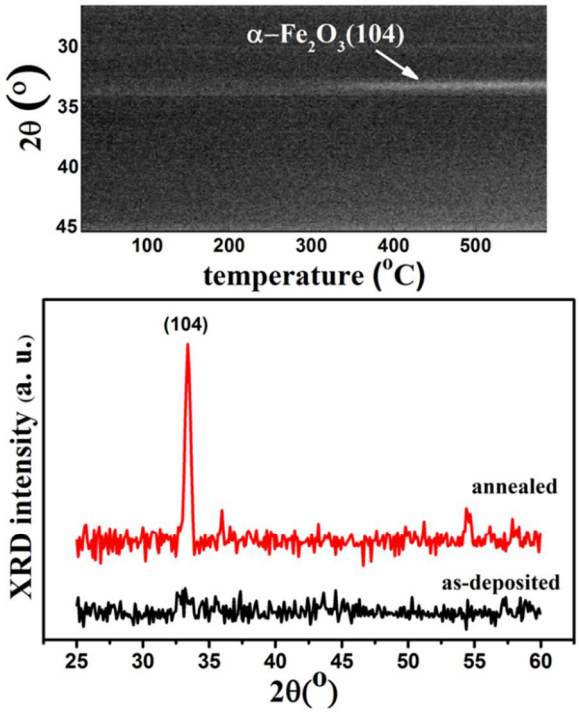

Figure 6. XRD patterns of a 26 nm thick Fe_2O_3 film deposited at 200 °C on a SiO_2 substrate and of the same film after annealing in He to 600 °C at a heating rate of 0.2 °C/s. The top figure shows the evolution of the XRD pattern during this thermal treatment.

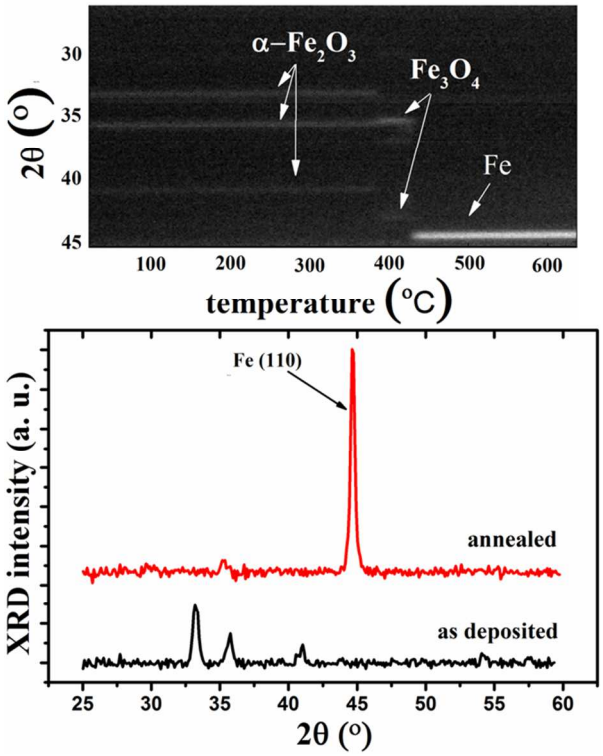

Figure 7. XRD patterns of a 28 nm thick Fe_2O_3 film deposited at 350 °C on a SiO_2 substrate and of the same film after annealing in H_2 to 650 °C at a heating rate of 0.2 °C/s. The top figure shows the evolution of the XRD pattern during this thermal treatment.

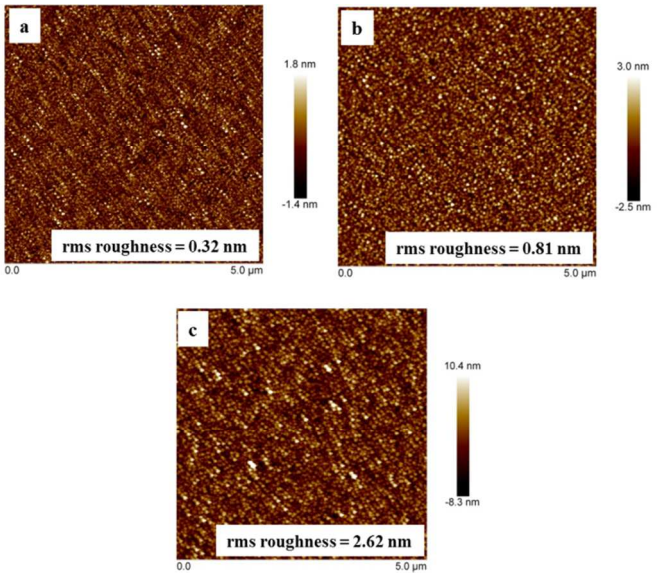

Figure 8. Atomic force micrographs of 13 nm thick Fe_2O_3 films (a) deposited at 200 °C, (b) the same annealed in He and (c) deposited at 350 °C on SiO_2 substrates.

Increase in the rms roughness value after annealing can be attributed to the formation of grains upon crystallization.

Conclusions

A new ALD process for the growth of uniform and pure α-Fe_2O_3 (hematite) thin films has been developed using t-butylferrocene as precursor and O_2 plasma as reactant. Both ALD half reactions are self-saturating in a broad temperature window ranging from 150 to 350 °C. Remarkably, the saturated growth rate increases with increasing temperature. Films deposited at 250 °C and higher temperatures are crystalline as-deposited, while the low temperature films can be crystallized by post-deposition annealing in He. Annealing in H_2 induces the formation of metallic iron. In comparison with most existing ALD processes for Fe_2O_3, this novel process enables deposition at temperatures as low as 150 °C, which is attractive for applications that require the controlled deposition of iron oxide on temperature sensitive materials. In future work, a detailed study of the growth behaviour on different substrates will be investigated.

Acknowledgements

This research was supported by the European Research Council (Starting Grant No. 239865), by the Flemish Research Foundation (FWO) and by the Special Research Fund BOF of Ghent University (GOA 01G01513).The authors also gratefully acknowledge Nico De Roo (UGent) for performing the XPS measurements.

Notes and references

1 S. Ohta and A. Terada, *Thin Solid Films*, 1986, **143**, 73–82
2 A. C. Sun, P. C. Kuo, C. Y. Chou, S. C. Chen, C. T. Lie, M. H. Lin, J. W. Chen, and H. L. Huang, *J. Magn. Magn. Mater.*, 2004, **272-276**, 1776–1777
3 Y. Huang, J. Lin, X. X. Ding, C. Tang, C. Z. Gu, and S. R. Qi, *Mater. Lett.*, 2007, **61**, 697–700
4 C. Park, D. Magana, and A. E. Stiegman, *Chem. Mater.*, 2007, **19**, 677–683
5 G. Carraro, D. Barreca, C. Maccato, E. Bontempi, L. E. Depero, C. de Julián Fernández, and A. Caneschi, *CrystEngComm*, 2013, **15**, 1039
6 K. Sirok, J. Jire, and L. Hudec, *Thin Solid Films*, 1994, **245**, 211–214
7 L. Huo, Q. Li, H. Zhao, L. Yu, S. Gao, and J. Zhao, *Sensors Actuators B*, 2005, **107**, 915–920
8 M. Aronniemi, J. Saino, and J. Lahtinen, *Thin Solid Films*, 2008, **516**, 6110–6115
9 G. Carraro, D. Barreca, E. Comini, A. Gasparotto, C. Maccato, C. Sada, and G. Sberveglieri, *CrystEngComm*, 2012, **14**, 6469
10 J. H. Kennedy and K. W. Frese, *J. Electrochem. Soc. Electrochem. Sci. Technol.*, 1978, **125**, 709–714
11 S. U. M. Khan and J. Akikusa, *J. Phys. Chem. B*, 1999, **103**, 7184–7189
12 N. Beermann, L. Vayssieres, S.-E. Lindquist, and A. Hagfeldt, *J. Electrochem. Soc.*, 2000, **147**, 2456–2461
13 A. Kay, I. Cesar, and M. Grätzel, *J. Am. Chem. Soc.*, 2006, **128**, 15714–21
14 V. satsangi, S. kumari, A. singh, R. shrivastav, and S. dass, *Int. J. Hydrogen Energy*, 2008, **33**, 312–318
15 G. Carraro, C. Maccato, A. Gasparotto, T. Montini, S. Turner, O. I. Lebedev, V. Gombac, G. Adami, G. Van Tendeloo, D. Barreca, and P. Fornasiero, *Adv. Funct. Mater.*, 2014, **24**, 372–378
16 W. Weiss, D. Zscherpel, and R. Schl, *Catal. Letters*, 1998, **52**, 215–220
17 O. Shekhah, W. Ranke, A. Schüle, G. Kolios, and R. Schlögl, *Angew. Chem. Int. Ed. Engl.*, 2003, **42**, 5760–3
18 W. Huang, W. Ranke, and R. Schlögl, *J. Phys. Chem. B*, 2005, **109**, 9202–4
19 A. Schüle, U. Nieken, O. Shekhah, W. Ranke, R. Schlögl, and G. Kolios, *Phys. Chem. Chem. Phys.*, 2007, **9**, 3619–34
20 L. Dghoughi, B. Elidrissi, C. Bernède, M. Addou, M. A. Lamrani, M. Regragui, and H. Erguig, *Appl. Surf. Sci.*, 2006, **253**, 1823–1829
21 J. Chavez-Galan and R. Almanza, *Sol. Energy*, 2007, **81**, 13–19
22 B. Mauvernay, L. Presmanes, S. Capdeville, V. G. de Resende, E. De Grave, C. Bonningue, and P. Tailhades, *Thin Solid Films*, 2007, **515**, 6532–6536
23 F. C. Voogt, T. Hibma, P. Smulders, and L. Niesen, *J. Cryst. Growth*, 1997, **174**, 440–445
24 Y. Gao, Y. Kim, and S. Chambers, *J. Mater. Res.*, 1998, **13**, 2003–2014
25 M. Gautier-soyer, S. Gota, E. Guiot, and M. Henriot, *Phys. Rev. B*, 1999, **60**, 14387–14395
26 B. Pal and M. Sharon, *Thin Solid Films*, 2000, **379**, 83–88
27 S. Trudel, C. H. W. Jones, and R. H. Hill, *J. Mater. Chem.*, 2007, **17**, 2206–2218
28 W. INGLERJR and S. KHAN, *Int. J. Hydrogen Energy*, 2005, **30**, 821–827
29 S. Park, S. Lim, and H. Choi, *Chem. Mater.*, 2006, **18**, 5150–5152
30 G. Carraro, D. Barreca, M. Cruz-Yusta, A. Gasparotto, C. Maccato, J. Morales, C. Sada, and L. Sánchez, *Chemphyschem*, 2012, **13**, 3798–801
31 D. Peeters, G. Carraro, C. Maccato, H. Parala, A. Gasparotto, D. Barreca, C. Sada, K. Kartaschew, M. Havenith, D. Rogalla, H.-W. Becker, and A. Devi, *Phys. Status Solidi A*, 2014, **211**, 316–322
32 M. Lie, H. Fjellvåg, and a. Kjekshus, *Thin Solid Films*, 2005, **488**, 74–81
33 K. Nielsch, J. Bachmann, M. Daub, J. Jing, M. Knez, U. Gösele, S. Barth, S. Mathur, J. Escrig, and D. Altbir, *ECS Trans.*, 2007, **11**, 139–148
34 J. Bachmann, J. Jing, M. Knez, S. Barth, H. Shen, S. Mathur, U. Gösele, and K. Nielsch, *J. Am. Chem. Soc.*, 2007, **129**, 9554–5
35 S. C. Riha, J. M. Racowski, M. P. Lanci, J. a Klug, A. S. Hock, and A. B. F. Martinson, *Langmuir*, 2013, **29**, 3439–45
36 M. Rooth, A. Johansson, K. Kukli, J. Aarik, M. Boman, and A. Hårsta, *Chem. Vap. Depos.*, 2008, **14**, 67–70
37 J. R. Scheffe, A. Francés, D. M. King, X. Liang, B. a. Branch, A. S. Cavanagh, S. M. George, and A. W. Weimer, *Thin Solid Films*, 2009, **517**, 1874–1879
38 A. Tamm, M. C. Dimri, J. Kozlova, A. Aidla, T. Tätte, T. Arroval, U. Mäeorg, H. Mändar, R. Stern, and K. Kukli, *J. Cryst. Growth*, 2012, **343**, 21–27

39 A. B. F. Martinson, M. J. DeVries, J. A. Libera, S. T. Christensen, J. T. Hupp, M. J. Pellin, and J. W. Elam, *J. Phys. Chem. C*, 2011, **115**, 4333–4339
40 J. a. Klug, N. G. Becker, S. C. Riha, A. B. F. Martinson, J. W. Elam, M. J. Pellin, and T. Proslier, *J. Mater. Chem. A*, 2013, **1**, 11607
41 X. . Zhang, G. . Wen, S. Huang, L. Dai, R. Gao, and Z. L. Wang, *J. Magn. Magn. Mater.*, 2001, **231**, 9–12
42 K. Aslan, M. Weisenberg, E. Hortle, and C. D. Geddes, *J. Appl. Phys.*, 2009, **106**, 014313
43 K. Aslan, Y. Zhang, and C. D. Geddes, *J. Phys. Chem. C*, 2009, **113**, 20535–20538
44 Y. Li, Y. Hu, G. Huang, and C. Li, *Particuology*, 2013, **11**, 460–467
45 Q. Xie, Y.-L. Jiang, C. Detavernier, D. Deduytsche, R. L. Van Meirhaeghe, G.-P. Ru, B.-Z. Li, and X.-P. Qu, *J. Appl. Phys.*, 2007, **102**, 083521
46 J. Musschoot, Q. Xie, D. Deduytsche, S. Van den Berghe, R. L. Van Meirhaeghe, and C. Detavernier, *Microelectron. Eng.*, 2009, **86**, 72–77
47 J. Dendooven, R. K. Ramachandran, K. Devloo-Casier, G. Rampelberg, M. Filez, H. Poelman, G. B. Marin, E. Fonda, and C. Detavernier, *J. Phys. Chem. C*, 2013, **117**, 20557–20561
48 W. Knaepen, C. Detavernier, R. L. Van Meirhaeghe, J. Jordan Sweet, and C. Lavoie, *Thin Solid Films*, 2008, **516**, 4946–4952
49 W. Knaepen, S. Gaudet, C. Detavernier, R. L. Van Meirhaeghe, J. J. Sweet, and C. Lavoie, *J. Appl. Phys.*, 2009, **105**, 083532
50 D. Longrie, K. Devloo-Casier, D. Deduytsche, S. Van den Berghe, K. Driesen, and C. Detavernier, *ECS J. Solid State Sci. Technol.*, 2012, **1**, Q123–Q129
51 I. J. M. Erkens, a. J. M. Mackus, H. C. M. Knoops, P. Smits, T. H. M. van de Ven, F. Roozeboom, and W. M. M. Kessels, *ECS J. Solid State Sci. Technol.*, 2012, **1**, P255–P262
52 S. M. George, *Chem. Rev.*, 2010, **110**, 111–31
53 A. J. M. Mackus, N. Leick, L. Baker, and W. M. M. Kessels, *Chem. Mater.*, 2012, **24**, 1752–1761
54 F. Visentin, R. Gerbasi, G. Rossetto, C. De Zorzi, C. S. Uniti, N. El Habra, D. Barreca, and A. Gasparotto, *Surf. Sci. spectra*, 2011, **18**, 29–35
55 T. Yamashita and P. Hayes, *Appl. Surf. Sci.*, 2008, **254**, 2441–2449

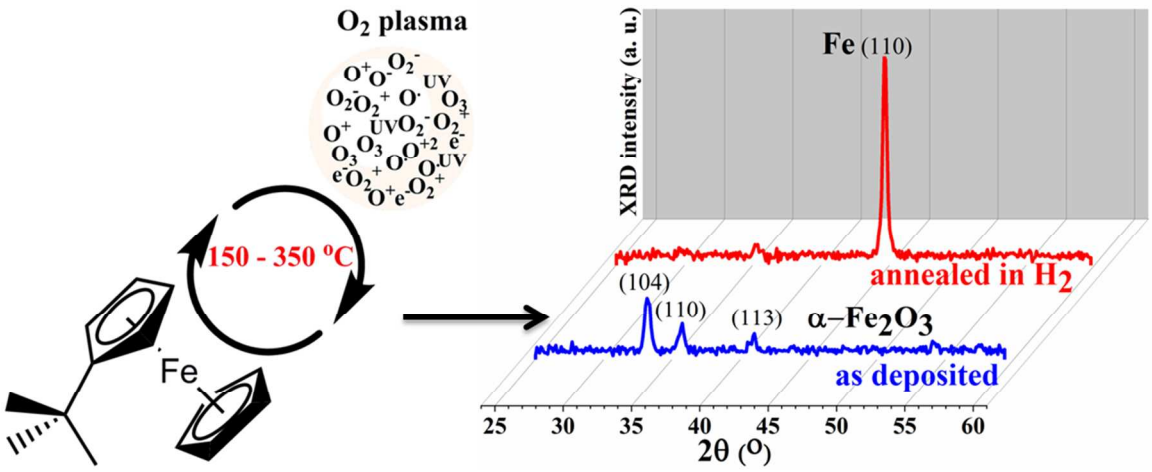

We demonstrate an ALD process for Fe_2O_3 that relies upon sequential pulsing of ter-Butyl ferrocene (TBF) and O_2 plasma and enables the deposition from temperatures as low as 150 °C.